Ceruloplasmin deficiency does not induce macrophagic iron overload: lessons from a new rat model of hereditary aceruloplasminemia

Moussa Kenawi, Emmanuel Rouger, Marie-Laure Island, Patricia Leroyer, François Robin, Séverine Remy, Laurent Tesson, Ignacio Anegon, Kevin Nay, Frédéric Derbré, et al.

Title

Ceruloplasmin deficiency does not induce macrophagic iron overload : lessons from a new rat model of hereditary aceruloplasminemia

Running title

Iron imbalance in hereditary aceruloplasminemia

Authors

Moussa Kenawi[1], Emmanuel Rouger[1], Marie-Laure Island[1], Patricia Leroyer[1], François Robin[1] Séverine Remy[2], Laurent Tesson[2], Ignacio Anegon[2], Kévin Nay[3], Frédéric Derbré[3], Pierre Brissot[1], Martine Ropert[1], Thibault Cavey[1], Olivier Loréal[1].

Affiliation

1- INSERM 1241, Univ Rennes, INRA1341, Platform Analyse Elémentaire et Métabolisme des Métaux, Institut NuMeCan (Nutrition Metabolisms and Cancer), CHU Pontchaillou, Rennes, France.
2- INSERM UMR 1064-CRTI, Transgenic Rats ImmunoPhenomic facility. 44093, Nantes, France
3- Laboratory "Movement, Sport, and Health Sciences" (M2S-EA7470), University Rennes 2-ENS Rennes, Bruz, France

Corresponding Author

Olivier Loréal, INSERM UMR 1241, Institut NuMeCan, Hôpital Pontchaillou, 35033 Rennes Cedex, France. Email : olivier.loreal@univ-rennes1.fr; tel : 33(2) 23 23 38 65

Abbreviations

Cp, ceruloplasmin ; HA, hereditary aceruloplasminemia ; *Hamp*, hepcidin antimicrobial peptide ; *Heph*, hephaestin ; *Hjv*, hemojuvelin BMP co-receptor ; LIC, liver iron concentration ; NTBI, non-transferrin bound iron ; SIC, spleen iron concentration ; *Slc11a2*, solute carrier family 11 member 2 ; *Slc39a14*, solute carrier family 39 member 14 ; *Slc40a1*, solute carrier family 40 member 1 ; *Tfrc*, transferrin receptor ; *Tfr2*, transferrin receptor 2 ; UIBC, unsaturated iron bound capacity.

Abstract

Hereditary aceruloplasminemia (HA) related to mutations in the ceruloplasmin gene leads to iron accumulation. Ceruloplasmin ferroxidase activity being considered essential for macrophage iron release, macrophage iron overload is expected, but is not found in hepatic and splenic macrophages in Humans. Our objective was to get a better understanding of the mechanisms leading to iron excess in HA.

A CRISPR/Cas9 knock-out of the *Cp* gene was performed on Sprague-Dawley rats. We evaluated the iron status in plasma, the expression of iron metabolism genes, and the status of other metals whose interactions with iron are increasingly recognized.

In $Cp^{-/-}$ rats, plasma ceruloplasmin and ferroxidase activity were absent, together with decreased iron concentration and transferrin saturation. Similarly to Humans, the hepatocytes were iron overloaded conversely to hepatic and splenic macrophages. Despite a relative hepcidin deficiency in $Cp^{-/-}$ rats and the loss of ferroxidase activity, potentially expected to limit the interaction of iron with transferrin, no increase of plasma non-transferrin bound iron level was found. Copper was decreased in the spleen while manganese was increased in the plasma.

These data suggest that the reported role of ceruloplasmin cannot fully explain the iron hepatosplenic phenotype in HA and encourage to search for additional mechanisms.

Key words

Iron overload ; ceruloplasmin ; hepcidin ; CRISPR/Cas9 ; genetic disease

Introduction

HA (OMIM # 604290) is a rare genetic disease affecting about one person per two millions (1). The disease is related to homozygous or compound heterozygous mutations within the ceruloplasmin gene (CP) located on chromosome 3 (2). HA is characterized by progressive iron overload targeting especially the liver and brain, and resulting in severe complications at variable ages, including diabetes and neurological disturbances (3–5). Despite iron overload, serum iron and transferrin saturation are low and anemia is also observed (3, 4).

The ceruloplasmin gene encodes the ceruloplasmin protein in two different forms resulting from an alternative splicing (6). The first gene product is mainly expressed by hepatocytes and secreted in plasma (7). The second one is characterized by the presence of a glycosylphosphatidylinositol sequence allowing its anchorage in plasmic membrane, especially in astrocytes according to in vitro studies (8). Ceruloplasmin is a multicopper-oxidase that catalyzes oxidation of ferrous iron into ferric iron (9). Ferroxidase activity requires the association of the peptidic sequence with six atoms of copper (7, 10). This biological activity is reported to play a key role in the iron release from cells, especially macrophages, providing iron to plasma for maintaining sufficient amounts of bio-available iron to the cells (11, 12). It has been reported that, following the iron release by the iron exporter ferroportin, ceruloplasmin permits, by oxidizing iron, its association to transferrin (9). Each transferrin molecule may link up to two iron atoms, and subsequently delivers iron to every cell in the body (9). Moreover, a role of GPI-ceruloplasmin in the stabilization of ferroportin on cell membrane has also been reported (13, 14).

Such a biological role suggests that, in HA, iron should be retained within macrophagic cells similarly to the reported findings in the ferroportin disease in which the activity of the iron exporter is strongly decreased (15, 16). Similarly, during inflammatory process characterized by high hepcidin levels, iron retention is observed within macrophages due to hepcidin increase (17, 18) that induces internalization and degradation of ferroportin (19, 20). However, from published HA case reports, it appears that, in the liver, the Kupffer cells are almost constantly spared by iron excess (4, 5, 21–23), and that, in the spleen, there is no increase of iron concentration (4, 5, 21, 22), contrasting with the observations in the ferroportin disease (15, 16).

Therefore, the hepatosplenic phenotype of iron overload observed in human HA does not fit with the reported biological role of ceruloplasmin, and our aim was to investigate the mechanisms contributing to iron misdistribution between spleen and liver, in order to progress in the understanding of the biological role of ceruloplasmin and of the mechanisms underlying the development of HA. It is noteworthy that ceruloplasmin knock-out mouse models give contrasted data regarding the iron overload phenotype in liver and spleen. Indeed, some animal data shows only hepatic iron overload, with no significant iron concentration increase in the spleen (24–26). Other reports describe both hepatic and splenic iron overload

(11, 27), with, in the liver, presence of iron within hepatic macrophages (11, 28). Thus, these data contrasts with the clinical findings in humans (4, 5, 21, 22), and suggests that mice could be not fully appropriate to mimic human HA. We hypothesized that a rat model could provide relevant informations to understand the disease ; thus, we used the rat as an alternative model to characterize the disease. We selected the Sprague-Dawley rat in which the type of hepatic iron load phenotype obtained during oral iron supplementation is very similar to the human profile both during genetic hemochromatosis and in excessive oral iron intake (29). Therefore, the CRISPR/Cas9 technology was used to generate and study a new rat aceruloplasminemic model aiming to mimic the unexpected human aceruloplasminemic hepato-splenic iron phenotype and to characterize the impact of aceruloplasminemia on other metals involved in biological processes (Cu, Zn, Mn, Mo, Co) that could play a role during aceruloplasminemia.

Material and Methods

Development of an aceruloplasminemic animal model

Sprague-Dawley (SD/Crl) rats were obtained from Charles River (L'Arbresle, France). All the animal care and procedures were approved by the Animal Experimentation Ethics Committee of the Pays de la Loire region, France, in accordance with the guidelines from the French National Research Council for the Care and Use of Laboratory Animals (Permit Number: CEEA-PdL-2015-692). The sgRNA was designed and produced by the facility TACGENE. The sgRNAcr377 used targeted the exon 1 of ceruloplasmin gene and had the following sequence : GGAATTACTGAAGCAGTTT. The sgRNA (200 ng/µl) and Cas9 protein (3µM) were incubated at room temperature for 10 min to allow formation of ribonucleoprotein complexes and then were kept at 4 °C until microinjection. Process and microinjection were performed as reported previously (30). Briefly, zygotes were collected from pre-pubescent (4–5 weeks old) SD donor female rats, super-ovulated by IP injection of pregnant mare serum gonadotropin (30 IU; Intervet, France) and 48h later, of human chorionic gonadotropin (20 IU; Intervet, France) that were mated with SD fertile males. One-cell-stage fertilized embryos were sequentially microinjected into the male pronucleus and into the cytoplasm. The same day, surviving embryos were implanted within pseudo-pregnant females (0.5 dpc) oviduct of and growed until full-term.

Genotyping

Tail biopsies from 8- to 10-day-old rats were digested overnight at 56 °C, in 500 µL of tissue digestion buffer (0.1M Tris-HCl pH 8.3, 5 mM EDTA, 0.2% SDS, 0.2M NaCl, 100 µg/ml proteinase K). The CRISPRs nuclease targeted regions were PCR amplified from diluted lysed samples (1/20) with a high-fidelity polymerase (Herculase II fusion polymerase). To detect gene edition, locus specific primers were used and mutations were analyzed by HMA-CE and direct sequencing of PCR products.

Characterization of aceruloplasminemic rats

From this founder, after crossing with wild-type SD rats, three groups (wild-type, heterozygotes, and homozygotes) of 10 rats each were obtained. The genotype of animals was performed by PCR using primers. DNA extractions were performed from young rat tails by using the Nucleospin Tissue® kit (Macherey Nagel), then dosed with Spectrometer ND-1000® (Nanodrop). PCR were realized by using 200 ng of DNA and by using specific primers: forward primer (GGGCTCCAAGAGGAAGAAAC), reverse primer (ATTTGGCCCATAAACAACAAAGAA), and GoTaq G2 Hot Start Green Mastermix® (Promega) on a Applied Biosystem Veriti 96 well Thermal Cycler® (ThermoFisher) with the following sequence : 3 minutes of heating at 95°C, followed by 30 cycles composed of 1 minute at 95°C, 1 minute at 62°C, and 2 minutes at 72°C, before a final single step at 72°C for 5 minutes. PCR products were investigated on 3%

agarose gel. Gels were exposed to U.V. in a transilluminator (Fisher scientific), and blots pictures were analyzed with Vision-Capt® software.

All studied animals were 6 month-old males. During breeding, animals were submitted at reversed lighting, had free access to water and standard rat food, and had benefited of litter changing one time a week. A standard diet, designed to support growth and maintenance (Teklad Global 16% protein Rodent Diet, Envigo, USA) contained 200 mg/kg of iron, 15 mg/kg of copper, 100 mg/kg of manganese, and 70 mg/kg of zinc. The protocol was validated by the Animal Experimentation Ethics Committee of Région Bretagne, France (referral number : 8554).

Animals were fasted 10 hours and anesthetized by isoflurane. After a laparotomy from symphysis to xiphoid appendix 1 ml of portal blood was collected. Then, cardiac blood sampling was performed in two successive phases : 1 ml on non-heparinized syringe and a larger volume on sodium-heparinate syringe respectively leading to cardiac arrest and animal death. The different organs were then collected, each one was rapidly split in two parts, and placed either in formaldehyde 4% or in liquid nitrogen.

Sample conditioning and storage

For serum preparation, after 2 hours at room temperature, non-heparinized blood samples were centrifuged (200 G; 10 minutes). Supernatants were collected, (centrifuged at 800 G ; 3 minutes), then aliquoted, and finally stored at -80°C until use.

For plasma preparation and erythrocytes cleaning, heparinized blood samples were centrifuged 10 minutes at 2230 G, (20°C). Supernatants were then collected and aliquoted in 100 µl to 600 µl samples, before storage at -80°C. Three to four ml of NaCl 0,9% were added for washing of blood cells pellets, then gently mixed to these last ones, and centrifuged at 1833 G during 10 minutes at 20°C. The washing was repeated three times. Then blood cells pellets were collected and aliquoted and immediately stored at -80°C.

Tissues collected in liquid nitrogen were stored at -80 °C.

Haemoglobin measurement

Haemoglobin concentration was measured in the clinical analysis platform of Rennes University Hospital, by a spectrophotometry method using an ABL 90® robot (Radiometer).

Biochemical assays

Plasma measurements were performed in the clinical analysis platform of Rennes University Hospital. Ceruloplasmin assays were performed by immunoturbidimetric method by a Cobas® 8000 robot (Roche), using a Ceruloplasmin 100 tests® kit (Roche) that contained a rabbit anti-human ceruloplasmin antibody. Serum and plasma iron concentrations, as well as unsaturated iron bound capacity (UIBC) values, were obtained by colorimetric method using respectively the kits Iron Gen.2, 750 tests® (Roche) and

Unsaturated Iron-Binding Capacity 100 tests® (Roche), both performed by a Cobas® 8000 robot (Roche) according to the principles previously reported (31). Transferrin saturation was calculated from UIBC value by the following equation : [iron/(iron+UIBC)]x100. Ferroxidase activity was measured on plasma samples by spectrophotometry using a Cobas® C111 robot (Roche), according to the method previously reported (32). Non-transferrin bound iron (NTBI) was quantified in serum rat samples by a previously reported method (33).

Quantification of metals in tissues and erythrocytes

For each tissue sample, a biopsy fragment of about 3 x 3 mm was cut and desiccated at 120°C during 10 to 15 hours. Samples were then recut for obtaining a weight between 0.5 and 3 mg. For erythrocytes, 250 µl of each sample were used. Assays were performed using ICP/MS apparatus equipped with a collision reaction cell as previously reported (31).

Histological analysis

Formaldehyde fixed biopsies were paraffin embedded. Four µm organ slices were performed and there stained by using Hemalun-eosin-safron and Perls methods in the H2P2 platform (UMS Biosit, Rennes).

Real-time qPCR

Total RNAs were extracted following the procedure of the Nucleospin RNA Plus® (Macherey Nagel) extraction kit, and then measured with Spectrometer ND-1000® (Nanodrop).

Reverse transcriptase step was performed by using the Hight Capacity cDNA Reverse Transcriptase® (Applied Biosystem) kit for obtaining 2 µg of cDNA per sample of 20 µl before a final 1/6 dilution in nuclease free water.

qPCRs were realized using 384 wells plates, with 2 µl of sample, 1 µl of forward primer then 1 µl of reverse primer, and 5 µl of SYBR GREEN 1 per well. Plates were then covered with a transparent film and centrifuged during 1 minute at 1000 rpm. Runs were performed in a 7900 HT Fast Real-time PCR system® (ThermoFisher) and data processed with SDS 2.4® software. Housekeeping genes used were *Hprt1*, *Tbp*, and *Gusb* ; Delta Ct were calculated by subtracting for each sample the Ct average of these three genes to the Ct of target gene. Primer pairs used are indicated in a Table *(Supp. data Table 1).*

Western-blotting

Cell membrane protein extraction was performed as previously reported, but at 100 000 g for one hour (34). Total protein extraction and western-blotting using 10 percent acrylamide gels were performed as described previously (35). The following antibodies were used : Ferroportin (1:500 ; Alomone Labs #

AIT001), p-SMAD1/5/8-Ser$^{463/465}$ (1:1000 ; Abcam # ab92698), p-STAT3-Tyr^{705} (1:1000 ; Cell Signaling # 9131), p-ERK1/2-Thr^{202}-Tyr^{204} (1:1000 ; Cell Signaling # 4376), Hephaestin (1:250 ; Abcam # ab108003), Hsc70 (1:5000 ; Santa Cruz # sc-7298). We used this p-ERK1/2-Thr202-Tyr204 antibody (36–41), as well as this p-STAT3-Tyr705 antibody (42–45), on the basis of their use in rats, as reported in the literature. We tested the p-SMAD1/5/8-Ser463/465 in human HepG2 hepatic cells that were exposed or not to BMP6, an inducer of SMAD1/5/8 phosphorylation (46). By western blot, we clearly found a signal increase at about 55 kDa in the sample treated by BMP6, compared to the untreated sample *(Data not shown)*. We tested the expression of ferroportin by western blot in spleen and liver samples and found a significant expression at the expected molecular weight close to 60 kDa ; the signal totally disappeared when the peptide used for immunization was added during antibody incubation. Regarding hephaestin, we analyzed rat spleen and liver and found, at the expected molecular weight (close to 130 kDa), a significant expression of the protein in the spleen, known to express hephaestin, and not in the liver that express very low levels of hephaestin mRNA (47, 48). The blot quantification analyses were conducted using Image Gauge® software (Fujifilm).

Statistical analysis

All the data were analyzed statistically with SPSS® software, using non-parametric tests. The three groups were submitted to Kruskal-Wallis test and Mann-Whitney test when appropriate. p values <0.05 were considered statistically significant. Data are presented as means ± SD.

Results

Generation of ceruloplasmin-deficient rats.

A sgRNA targeting exon 1 of the ceruloplasmin (*Cp*) gene *(Fig.1 A and B)* was designed, then microinjected complexed with Cas9 in rat zygotes (n=189) and implanted (n=154) in pseudopregnant females. Offspring (n=47) were genotyped and resulted in the generation of mutated animals (n=30) with different types in insertions and deletions *(Data not shown)*. Among these mutated rats, one of them showed a mutation that resulted in a 54 base pair deletion and a 2 base pair insertion in exon 1 of the ceruloplasmin gene *(Fig.1 C)*. This resulted in the disruption of the coding frame and the appearance of a premature stop codon occurring in exon 2 *(Fig.1 D)* with a predicted degradation of the whole mRNA due to the widely distributed mechanism of nonsense-mediated mRNA decay (49).

This founder animal was crossed with wild-type animals and the mutation was observed in the F1 offspring. F1 heterozygous mutated animals were crossed to obtain homozygous mutated animals *(Fig.1 E)*.

Characterisation of the iron phenotype in aceruloplasminemic rat model

Plasma ceruloplasmin assays showed very low ceruloplasmin concentrations in homozygotes, and significantly lowered values in heterozygotes compared to wild-type rats *(Fig.2 A)*. Ferroxidase activity was almost undetectable in homozygotes, and half preserved in heterozygote animals *(Fig.2 B)*.

Plasma iron concentration was significantly decreased in homozygotes and fully preserved in heterozygotes compared to wild-types, both in peripheral and portal plasma *(Fig.2 C and D)*. Transferrin saturation followed the same variations *(Fig.2 E and F)*. NTBI levels were decreased both in portal and systemic plasma in homozygotes as compared to wild-types and heterozygotes *(Fig.2 G and H)*.
Hemoglobin concentrations were not affected in homozygous and heterozygous groups as compared to controls, and erythrocyte iron concentration was not modified by the presence of the mutation at heterozygous or homozygous state *(Fig.2 I and J)*.

Liver iron concentration (LIC) was significantly higher in homozygous rats, whereas spleen iron concentration (SIC) was significantly lower compared to values found in wild-type animals ; in heterozygous rats, both LIC and SIC were not affected compared to wild-type animals *(Fig.2 K and L)*.

Perls staining showed liver iron deposits in homozygotes, located in hepatocytes and sparing Kupffer cells *(Fig.3 A and B)*. Spleen iron deposits, mainly located in macrophages from the red pulp, appeared to be lower in homozygotes than in wild-type animals *(Fig.3 C and D)*.

Characterization of the non-iron metal phenotype in aceruloplasminemic rats

Plasma copper concentrations were strongly decreased in homozygotes, and half preserved in heterozygotes, while erythrocyte copper concentrations were not affected in mutated animals *(Fig.4 A and*

B). Liver copper concentration was unchanged, while spleen copper was significantly lower in homozygotes and heterozygotes compared to wild-type animals *(Fig.4 C and D)*.

Concentrations of other metals including molybdenum, manganese, zinc and cobalt were also investigated in liver, spleen, erythrocytes and plasma of animals *(Supp. data Table 2)*. In homozygous animals, a significant increase of cobalt and manganese concentrations was found in erythrocytes and plasma, as compared to heterozygous and controls *(Fig.4 E and F)*.

Impact of aceruloplasminemia on the expression of iron metabolism genes

In the liver, hepcidin antimicrobial peptide (*Hamp*) mRNA levels were slightly but significantly decreased in homozygous as compared to heterozygous animals, but not versus wild-type rats *(Fig.5 A)*. The ratio between *Hamp* mRNA and LIC levels was strongly decreased in homozygous animals as compared to wild-type and heterozygous animals *(Fig.5 B)*. Hepatic mRNA levels of transferrin receptor 2 (*Tfr2*), hemojuvelin BMP co-receptor (*Hjv*), and *Hfe, (Supp. data Figure 1)* did not change between the groups. Levels of phosphorylated forms of ERK1/2, STAT3, and SMAD1/5/8, proteins did not show significant variations between wild-type and homozygous animals *(Fig.5 C ; Supp. data Figure 2)*. Transferrin receptor (*Tfrc*), solute carrier family 11 member 2 (*Slc11a2*), solute carrier family 39 member 14 (*Slc39a14*) *(Supp. Data Figure 1),* solute carrier family 40 member 1 (*Slc40a1*) and hephaestin (*Heph*) *(Fig.5 D and E)* mRNA levels, were not affected in homozygous and heterozygous animals. It is noteworthy that hepatic *Heph* mRNA levels were particularly low in all groups. The hepatic expression of cell membrane ferroportin was not significantly modulated in aceruloplasminemic rats *(Fig.5 F ; Supp. data Figure 2)*. Hephaestin cell membrane protein was undetectable both in wild-type and homozygous groups in the liver *(data not shown)*.

In the spleen, the mRNA levels of *Tfrc, Slc11a2 (Supp. Data Figure 1)*, and *Heph (Fig.5 H)*, were not different between the three groups. mRNA levels of *Slc40a1*, were slightly but significantly increased in homozygous as compared to wild-type animals, only *(Fig.5 G)*. Ferroportin and hephaestin cell membrane protein expression were not significantly modulated in homozygous animals *(Fig.5 I ; Supp. data Figure 2)*.

In the duodenum, mRNA levels of *Slc11a2 (Supp. data Figure 1)*, *Slc40a1* and *Heph (Fig.5 J and K)* were not affected by homozygous or heterozygous state. Ferroportin and hephaestin cell membrane protein expression were unchanged between wild-type and homozygous animals *(Fig.5 L ; Supp. data Figure 2)*.

Impact of aceruloplasminemia on the expression of copper metabolism genes

Hepatic mRNA levels of the two genes encoding factor V and factor VIII that are multicopper oxidases were unchanged in homozygous and heterozygous animals, compared to controls *(Supp. data Figure 3)*. mRNA levels of *Atp7a*, *Atp7b*, and *Slc31a1* genes that encode copper transporters were unchanged in both liver and spleen *(Supp. data Figure 3)*.

Discussion

Our data, obtained in a new aceruloplasminemic rat model, shows that serum biochemical parameters obtained in the *Cp*$^{-/-}$ were in accordance with those reported in humans (4, 5) and in one mouse model (50). Indeed, both ceruloplasmin and ferroxidase activity were undetectable. Moreover, plasma iron concentration and transferrin saturation levels were significantly decreased in homozygous animals only, supporting a strong decrease of plasma iron bioavailability. Importantly, there were neither anemia nor reduction of erythrocyte iron content in our model, in contrast with human findings (4, 22, 51) and some mouse models (28, 52, 53), but in accordance with another mouse model (11).

Our findings with, in the liver, a highly predominant hepatocyte iron overload, and, in the spleen, a decrease of iron concentration, fully fit the human disease (4, 5, 21, 22), whereas data obtained in mice are very contrasted (11, 24–28). We must underline that in mice, the genetic background in inbred strains plays a major role as a modifier of the iron phenotype (54, 55). Conversely, our data have been obtained in an outbred strain that keeps a significant genetic background variability that may help to identify strong elements involved in the development of the phenotype (56). Indeed, it has been recently reported that for most applications in animal studies, the use of robust and diverse subjects is preferred to obtain generalizable conclusions across conditions and populations (57). It has been proposed that, contrary to classical expectations, the adoption of outbred animals as research subjects may improve experimental replicability (57). Moreover, it should be outlined that, conversely to rats and Humans, in mice, iron deposits during iron overload may be localized in the nucleus of hepatocytes, suggesting significant differences in the iron metabolism of mouse hepatocytes (58). In addition, there is only one gene of hepcidin in rats like in Humans, in contrast with mice that exhibit two genes, the role of the second one being not yet clearly established (59, 60). Therefore, we thought that a rat model would be valuable to get complementary and relevant informations for a better understanding of ceruloplasmin functions involved in HA.

Our histological data, as reported in Humans (4, 5, 21, 22), showing that iron deposits are mainly located in hepatocytes whereas both Kupffer cells, the resident macrophages in the liver, and spleen macrophages did not exhibit significant iron deposits compared to controls, contrast with the classical pathophysiological hypothesis postulating iron retention in macrophages during HA (13). Our data strongly suggests that, during HA, iron is not retained within macrophage despite the strong decrease of ferroxidase activity. These findings contrast with those in mice showing that iron egress is decreased in macrophages when ferroxidase activity is altered (27). However, they are in agreement with other mouse reports (24–26), suggesting that iron egress is not altered in macrophages.

Therefore, complementary mechanisms contributing to the hepatocyte iron load must be searched. During genetic hemochromatosis, the archetype of hepatocyte iron overload, the following mechanistic sequence is involved in the iron loading process : hepcidin deficiency, related to mutations in the *Hfe* gene, but also in *Hjv*, *Hamp* or *Tfr2* genes, leads to an increase of transferrin saturation with appearance of NTBI (61), quickly taken up by hepatocytes through the ZIP 14 protein (62).

Our data shows that the homozygous $Cp^{-/-}$ animals presented a relative hepcidin deficiency, as indicated by a drop of the hepcidin on LIC ratio, reflecting the absence of the expected increase of hepcidin mRNA levels in the liver of iron overloaded animals. Moreover, we did not find any modulation of *Hfe*, *Hjv* and *Tfr2* hepatic mRNA steady-state levels that could have participated to the genesis of the relative hepcidin deficient state. In addition, the transduction pathways that depend on these genes did not seem affected as suggested by the absence of phosphorylation level decrease of ERK1/2, SMAD1/5/8 and STAT3. Whether an inhibitory signal resulting from an erythropoietic effect of the disease is involved, even in absence of anemia, deserves further investigation. It is noteworthy that, whereas the expression of the iron exporter ferroportin, (the hepcidin target) on cell membrane has been reported in cell models to be impaired in macrophages in case of ceruloplasmin deficiency (13, 14, 63), we did not find any modulation of ferroportin mRNA and protein levels in the spleen, that is particularly rich in macrophages, and in the liver.

Ferroxidase activity being reported as required for the iron association to transferrin (64), we looked for an increase of NTBI in the serum of homozygous animals, despite the absence of transferrin saturation increase. Similarly to what has been reported in Humans (4), we did not find any NTBI increase not only in systemic blood flow, but also in portal flow that receives iron from spleen and digestive tract. Moreover, the mRNA levels of *Slc39a14*, the specific transporter of NTBI (62), was not modulated in the liver of $Cp^{-/-}$ animals. Taken together, these data suggests that (an) alternative mechanism(s) allow(s) the transfer of iron on transferrin. In this context, it is noteworthy that the expression level of hephaestin that could be involved in a compensation of ceruloplasmin deficiency was not significantly increased in the spleen and in the duodenum in aceruloplasminemic rats. Moreover, the ferroportin expression level was not affected in spleen, liver and duodenum.

Finally, considering strong relationships between ceruloplasmin and Cu and previous reports underlying potential interactions between the metabolism of iron and those of other metals (65), we investigated the concentration of these metals in plasma and tissues in order to identify elements that could play a role in the development of the disease. We therefore explored whether aceruloplasminemic condition modulated the concentrations of Cu, Mn, Zn Co, Mo in liver, spleen, erythrocytes, and plasma.

The multicopper-oxidase, ceruloplasmin is the most important carrier of Cu in plasma, described as containing about 93 percent of this metal (66), in accordance with lowered plasma copper concentrations in HA patients (4, 5, 22, 51), and with animal data (25). Therefore, as expected, we found a strong decrease of

plasma Cu in aceruloplasminemic animals. Regarding the liver, HA case reports are not univocal on copper concentrations, that have been found stable (22) or increased (3), As previously described in HA mice models (25, 28), liver copper concentrations in our $Cp^{-/-}$ rats did not show any significant variations. However, we found a decrease of spleen copper concentrations in $Cp^{-/-}$ and $Cp^{+/-}$ animals compared to wild-type rats, contrasting with a previous report in HA mice (25). It should be noted that this variation affected both $Cp^{-/-}$ and $Cp^{+/-}$ animals, whereas, when analyzing plasma and tissue iron parameters, significant variations were only found in $Cp^{-/-}$ animals. Therefore, it can be hypothesized that the decrease of ceruloplasmin is involved in the spleen copper decrease. This decrease in spleen copper content does not seem related to a lowered copper entry into spleen macrophages during the erythrophagocytosis process, as suggested by the equal erythrocyte copper contents between the three groups.

It is noteworthy that in $Cp^{-/-}$ animals, the plasma manganese levels were found to be increased. The role of ferroportin in Mn egress being supported by previous data (65), this observation supports the absence of direct effect of ceruloplasmin on metal egress. Interestingly, we did not find an overexpression of hephaestin that could have compensated the absence of ceruloplasmin in the spleen, both at mRNA and protein levels.

Whether these alterations play a role during HA will require further investigations.

In conclusion, this new aceruloplasminemic rat model mimics the human hepatosplenic iron load phenotype during HA. Our data suggests that iron overload in this disease is not primarily related to iron retention within macrophages. Whether hepcidin deficiency plays, despite the absence of NTBI, a role in the development of hepatocyte iron load remains to be clarified. Elucidation of the mechanisms involved in these iron metabolism disturbances could help to further understand how iron develops in the brain of human aceruloplasminemia, causing devastating complications.

Acknowledgements

This work was supported by the “Fondation maladies rares”, the “Région Bretagne” (MK), INSERM and AFeMER. This work was partially supported by the “TEFOR” project funded by the « Investissements d’Avenir » French Government program (ANRII-INSB-0014), and also member of “CELPHEDIA” infrastructure. This work was realized in the context of the Labex IGO project (ANR-11-LABX-0016-01) and the IHU-Cesti project (ANR-10-IBHU-005) which both are part of the « Investissements d’Avenir » French Government program. The IHU-Cesti project is also supported by Nantes Métropole and Région Pays de la Loire. The author’s thanks the U1154-UMR7196 TACGENE for design and produce the sgRNA.

Author's contributions

M. Kenawi performed experiments, collected and analyzed the data, and wrote the manuscript. E. Rouger, M. L. Island, P. Leroyer, F. Robin, K. Nay, F. Derbré, M. Ropert, and T. Cavey performed research experiments and corrected the manuscript. S. Rémy and L. Tesson designed and performed research experiments, collected and analyzed data. I. Anegon supervised research and partially wrote the manuscript. P. Brissot contributed to design the study, to analyze the data, and to write the manuscript. O. Loréal designed the study, contributed to the experiment, analyzed the data and wrote the manuscript.

References

1. Miyajima, H. (2015) Aceruloplasminemia. *Neuropathology* **1**, 83–90
2. Yang, F., Naylor, S. L., Lum, J. B., Cutshaw, S., McCombs, J. L., Naberhaus, K. H., McGill, J. R., Adrian, G. S., Moore, C. M., and Barnett, D. R. (1986) Characterization, mapping, and expression of the human ceruloplasmin gene. *Proc. Natl. Acad. Sci.* **83**, 3257–3261
3. Bosio, S., De Gobbi, M., Roetto, A., Zecchina, G., Leonardo, E., Rizzetto, M., Lucetti, C., Petrozzi, L., Bonuccelli, U., and Camaschella, C. (2002) Anemia and iron overload due to compound heterozygosity for novel ceruloplasmin mutations. *Blood* **100**, 2246–2248
4. Loréal, O., Turlin, B., Pigeon, C., Moisan, A., Ropert, M., Morice, P., Gandon, Y., Jouanolle, A.-M., Vérin, M., and Hider, R. C. (2002) Aceruloplasminemia: new clinical, pathophysiological and therapeutic insights. *J. Hepatol.* **36**, 851–856
5. Finkenstedt, A., Wolf, E., Höfner, E., Gasser, B. I., Bösch, S., Bakry, R., Creus, M., Kremser, C., Schocke, M., and Theurl, M. (2010) Hepatic but not brain iron is rapidly chelated by deferasirox in aceruloplasminemia due to a novel gene mutation. *J. Hepatol.* **53**, 1101–1107
6. Patel, B. N., Dunn, R. J., and David, S. (2000) Alternative RNA splicing generates a glycosylphosphatidylinositol-anchored form of ceruloplasmin in mammalian brain. *J. Biol. Chem.* **275**, 4305–4310
7. Sato, M. and Gitlin, J. (1991) Mechanisms of copper incorporation during the biosynthesis of human ceruloplasmin. *J. Biol. Chem.* **266**, 5128–5134
8. Patel, B. N. and David, S. (1997) A novel glycosylphosphatidylinositol-anchored form of ceruloplasmin is expressed by mammalian astrocytes. *J. Biol. Chem.* **272**, 20185–20190
9. Osaki, S., Johnson, D. A., and Frieden, E. (1966) The possible significance of the ferrous oxidase activity of ceruloplasmin in normal human serum. *J. Biol. Chem.* **241**, 2746–2751
10. Hellman, N. E., Kono, S., Mancini, G. M., Hoogeboom, A., De Jong, G., and Gitlin, J. D. (2002) Mechanisms of copper incorporation into human ceruloplasmin. *J. Biol. Chem.* **277**, 46632–46638
11. Harris, Z., Durley, A., Man, T., and Gitlin, J. (1999) Targeted gene disruption reveals an essential role for ceruloplasmin in cellular iron efflux. *Proc. Natl. Acad. Sci. U. S. A.* **96**, 10812
12. Young, S., Fahmy, M., and Golding, S. (1997) Ceruloplasmin, transferrin and apotransferrin facilitate iron release from human liver cells. *FEBS Lett.* **411**, 93
13. De Domenico, I., Ward, D. M., Di Patti, M. C. B., Jeong, S. Y., David, S., Musci, G., and Kaplan, J. (2007) Ferroxidase activity is required for the stability of cell surface ferroportin in cells expressing GPI-ceruloplasmin. *EMBO J.* **26**, 2823–2831
14. Kono, S., Yoshida, K., Tomosugi, N., Terada, T., Hamaya, Y., Kanaoka, S., and Miyajima, H. (2010) Biological effects of mutant ceruloplasmin on hepcidin-mediated internalization of ferroportin. *Biochim. Biophys. Acta BBA - Mol. Basis Dis.* **1802**, 968–975
15. Pietrangelo, A. (2004) The ferroportin disease. *Blood Cells. Mol. Dis.* **32**, 131–138
16. Pietrangelo, A. (2017) Ferroportin disease: pathogenesis, diagnosis and treatment. *Haematologica* **102**, 1972–1984
17. Nemeth, E., Rivera, S., Gabayan, V., Keller, C., Taudorf, S., Pedersen, B. K., and Ganz, T. (2004) IL-6 mediates hypoferremia of inflammation by inducing the synthesis of the iron regulatory hormone hepcidin. *J. Clin. Invest.* **113**, 1271–1276
18. Wrighting, D. M. and Andrews, N. C. (2006) Interleukin-6 induces hepcidin expression through STAT3. *Blood* **108**, 3204
19. De Domenico, I., Ward, D. M., Langelier, C., Vaughn, M. B., Nemeth, E., Sundquist, W. I., Ganz, T., Musci, G., and Kaplan, J. (2007) The Molecular Mechanism of Hepcidin-mediated Ferroportin Down-Regulation. *Mol. Biol. Cell* **18**, 2569
20. Theurl, I., Theurl, M., Seifert, M., Mair, S., Nairz, M., Rumpold, H., Zoller, H., Bellmann-Weiler, R., Niederegger, H., and Talasz, H. (2008) Autocrine formation of hepcidin induces iron retention in human monocytes. *Blood* **111**, 2392–2399

21. Skidmore, F., Drago, V., Foster, P., Schmalfuss, I., Heilman, K., and Streiff, R. (2008) Aceruloplasminaemia with progressive atrophy without brain iron overload: treatment with oral chelation. *J Neurol Neurosurg Psychiatry* **79**, 467–470
22. Kono, S., Suzuki, H., Takahashi, K., Takahashi, Y., Shirakawa, K., Murakawa, Y., Yamaguchi, S., and Miyajima, H. (2006) Hepatic iron overload associated with a decreased serum ceruloplasmin level in a novel clinical type of aceruloplasminemia. *Gastroenterology* **131**, 240–245
23. Piperno, A. and Alessio, M. (2018) Aceruloplasminemia: waiting for an efficient therapy. *Front. Neurosci.* **12**, 903
24. Jiang, R., Hua, C., Wan, Y., Jiang, B., Hu, H., Zheng, J., Fuqua, B., Dunaief, J., Anderson, G., and David, S. (2015) Hephaestin and ceruloplasmin play distinct but interrelated roles in iron homeostasis in mouse brain. *J. Nutr.* **145**, 1003
25. Meyer, L. A., Durley, A. P., Prohaska, J. R., and Harris, Z. L. (2001) Copper transport and metabolism are normal in aceruloplasminemic mice. *J. Biol. Chem.* **276**, 36857–36861
26. Gouya, L., Muzeau, F., Robreau, A., Letteron, P., Couchi, E., Lyoumi, S., Deybach, J., Puy, H., Fleming, R., and Demant, P. (2007) Genetic study of variation in normal mouse iron homeostasis reveals ceruloplasmin as an HFE-hemochromatosis modifier gene. *Gastroenterology* **132**, 679–686
27. Chen, H., Attieh, Z. K., Gao, H., Huang, G., Su, T., Ke, W., and Vulpe, C. D. (2009) Age-related changes in iron homeostasis in mouse ferroxidase mutants. *Biometals* **22**, 827
28. Yamamoto, K., Yoshida, K., Miyagoe, Y., Ishikawa, A., Hanaoka, K., Nomoto, S., Kaneko, K., Ikeda, S., and Takeda, S. (2002) Quantitative evaluation of expression of iron-metabolism genes in ceruloplasmin-deficient mice. *Biochim. Biophys. Acta* **1588**, 195
29. Bacon, B. R., Tavill, A. S., Brittenham, G. M., Park, C., and Recknagel, R. (1983) Hepatic lipid peroxidation in vivo in rats with chronic iron overload. *J. Clin. Invest.* **71**, 429–439
30. Remy, S., Chenouard, V., Tesson, L., Usal, C., Ménoret, S., Brusselle, L., Heslan, J.-M., Nguyen, T. H., Bellien, J., and Merot, J. (2017) Generation of gene-edited rats by delivery of CRISPR/Cas9 protein and donor DNA into intact zygotes using electroporation. *Sci. Rep.* **7**, 16554
31. Cavey, T., Ropert, M., de Tayrac, M., Bardou-Jacquet, E., Island, M., Leroyer, P., Bendavid, C., Brissot, P., and Loréal, O. (2015) Mouse genetic background impacts both on iron and non-iron metals parameters and on their relationships. *Biometals Int. J. Role Met. Ions Biol. Biochem. Med.* **28**, 733
32. Lainé, F., Ropert, M., Le Lan, C., Loréal, O., Bellissant, E., Jard, C., Pouchard, M., Le Treut, A., and Brissot, P. (2002) Serum ceruloplasmin and ferroxidase activity are decreased in HFE C282Y homozygote male iron-overloaded patients. *J. Hepatol.* **36**, 60–65
33. Breuer, W. and Cabantchik, Z. (2001) A fluorescence-based one-step assay for serum non-transferrin-bound iron. *Anal. Biochem.* **299**, 194
34. Canonne-Hergaux, F., Gruenheid, S., Ponka, P., and Gros, P. (1999) Cellular and subcellular localization of the Nramp2 iron transporter in the intestinal brush border and regulation by dietary iron. *Blood* **93**, 4406–4417
35. Salaun, E., Lefeuvre-Orfila, L., Cavey, T., Martin, B., Turlin, B., Ropert, M., Loreal, O., and Derbré, F. (2015) Myriocin prevents muscle ceramide accumulation but not muscle fiber atrophy during short-term mechanical unloading. *J. Appl. Physiol.* **120**, 178–187
36. Cornejo, P., Varela, P., Videla, L. A., and Fernández, V. (2005) Chronic iron overload enhances inducible nitric oxide synthase expression in rat liver. *Nitric Oxide* **13**, 54–61
37. Chen, L., Xiong, S., She, H., Lin, S. W., Wang, J., and Tsukamoto, H. (2007) Iron causes interactions of TAK1, p21ras, and phosphatidylinositol 3-kinase in caveolae to activate IκB kinase in hepatic macrophages. *J. Biol. Chem.* **282**, 5582–5588
38. Zhang, Y., Cheng, Y., Wang, N., Zhang, Q., and Wang, K. (2014) The action of JAK, SMAD and ERK signal pathways on hepcidin suppression by polysaccharides from Angelica sinensis in rats with iron deficiency anemia. *Food Funct.* **5**, 1381–1388
39. Poli, M., Luscieti, S., Gandini, V., Maccarinelli, F., Finazzi, D., Silvestri, L., Roetto, A., and Arosio, P. (2010) Transferrin receptor 2 and HFE regulate furin expression via mitogen-activated protein kinase/extracellular signal-regulated kinase (MAPK/Erk) signaling. Implications for transferrin-dependent hepcidin regulation. *Haematologica* **95**, 1832–1840

40. Tangudu, N. K., Buth, N., Strnad, P., Cirstea, I. C., and Spasić, M. V. (2019) Deregulation of Hepatic Mek1/2–Erk1/2 Signaling Module in Iron Overload Conditions. *Pharmaceuticals* **12**, 70
41. Wallace, D. F., Summerville, L., Crampton, E. M., Frazer, D. M., Anderson, G. J., and Subramaniam, V. N. (2009) Combined deletion of Hfe and transferrin receptor 2 in mice leads to marked dysregulation of hepcidin and iron overload. *Hepatology* **50**, 1992–2000
42. Cavey, T., Pierre, N., Nay, K., Allain, C., Ropert, M., Loréal, O., and Derbré, F. (2017) Simulated microgravity decreases circulating iron in rats: role of inflammation-induced hepcidin upregulation. *Exp. Physiol.* **102**, 291–298
43. Armitage, A. E., Eddowes, L. A., Gileadi, U., Cole, S., Spottiswoode, N., Selvakumar, T. A., Ho, L.-P., Townsend, A. R., and Drakesmith, H. (2011) Hepcidin regulation by innate immune and infectious stimuli. *Blood* **118**, 4129–4139
44. De Domenico, I., Zhang, T. Y., Koening, C. L., Branch, R. W., London, N., Lo, E., Daynes, R. A., Kushner, J. P., Li, D., and Ward, D. M. (2010) Hepcidin mediates transcriptional changes that modulate acute cytokine-induced inflammatory responses in mice. *J. Clin. Invest.* **120**, 2395–2405
45. Huang, H., Constante, M., Layoun, A., and Santos, M. M. (2009) Contribution of STAT3 and SMAD4 pathways to the regulation of hepcidin by opposing stimuli. *Blood* **113**, 3593–3599
46. Kersten, C., Sivertsen, E. A., Hystad, M. E., Forfang, L., Smeland, E. B., and Myklebust, J. H. (2005) BMP-6 inhibits growth of mature human B cells; induction of Smad phosphorylation and upregulation of Id1. *BMC Immunol.* **6**, 9
47. LI, Y. Q., Bin, B., Zheng, Q. Q., Hong, Y., and Zhuang, G. H. (2013) Quantitative study of iron metabolism-related genes expression in rat. *Biomed. Environ. Sci.* **26**, 808–819
48. Zhang, A.-S., Xiong, S., Tsukamoto, H., and Enns, C. A. (2004) Localization of iron metabolism–related mRNAs in rat liver indicate that HFE is expressed predominantly in hepatocytes. *Blood* **103**, 1509–1514
49. Frischmeyer, P. A. and Dietz, H. C. (1999) Nonsense-mediated mRNA decay in health and disease. *Hum. Mol. Genet.* **8**, 1893–1900
50. Guo, P., Cui, R., Chang, Y.-Z., Wu, W.-S., Qian, Z.-M., Yoshida, K., Qiao, Y.-T., Takeda, S., and Duan, X.-L. (2009) Hepcidin, an antimicrobial peptide is downregulated in ceruloplasmin-deficient mice. *Peptides* **30**, 262–266
51. Ogimoto, M., Anzai, K., Takenoshita, H., Kogawa, K., Akehi, Y., Yoshida, R., Nakano, M., Yoshida, K., and Ono, J. (2011) Criteria for early identification of aceruloplasminemia. *Intern. Med.* **50**, 1415–1418
52. Cherukuri, S., Tripoulas, N. A., Nurko, S., and Fox, P. L. (2004) Anemia and impaired stress-induced erythropoiesis in aceruloplasminemic mice. *Blood Cells. Mol. Dis.* **33**, 346–355
53. Fuqua, B. K., Lu, Y., Frazer, D. M., Darshan, D., Wilkins, S. J., Dunn, L., Loguinov, A. V., Kogan, S. C., Matak, P., and Chen, H. (2018) Severe iron metabolism defects in mice with double knockout of the multicopper ferroxidases hephaestin and ceruloplasmin. *Cell. Mol. Gastroenterol. Hepatol.* **6**, 405–427
54. Dupic, F., Fruchon, S., Bensaid, M., Borot, N., Radosavljevic, M., Loreal, O., Brissot, P., Gilfillan, S., Bahram, S., and Coppin, H. (2002) Inactivation of the hemochromatosis gene differentially regulates duodenal expression of iron-related mRNAs between mouse strains. *Gastroenterology* **122**, 745–751
55. Dupic, F., Fruchon, S., Bensaid, M., Loreal, O., Brissot, P., Borot, N., Roth, M., and Coppin, H. (2002) Duodenal mRNA expression of iron related genes in response to iron loading and iron deficiency in four strains of mice. *Gut* **51**, 648–653
56. Brower, M., Grace, M., Kotz, C. M., and Koya, V. (2015) Comparative analysis of growth characteristics of Sprague Dawley rats obtained from different sources. *Lab. Anim. Res.* **31**, 166–173
57. Tuttle, A. H., Philip, V. M., Chesler, E. J., and Mogil, J. S. (2018) Comparing phenotypic variation between inbred and outbred mice. *Nat. Methods* **15**, 994
58. Smith, A. G., Carthew, P., Francis, J. E., Edwards, R. E., and Dinsdale, D. (1990) Characterization and accumulation of ferritin in hepatocyte nuclei of mice with iron overload. *Hepatology* **12**, 1399–1405
59. Ilyin, G., Courselaud, B., Troadec, M.-B., Pigeon, C., Alizadeh, M., Leroyer, P., Brissot, P., and Loréal, O. (2003) Comparative analysis of mouse hepcidin 1 and 2 genes: evidence for different patterns of expression and co-inducibility during iron overload. *FEBS Lett.* **542**, 22–26

60. Courselaud, B., Troadec, M.-B., Fruchon, S., Ilyin, G., Borot, N., Leroyer, P., Coppin, H., Brissot, P., Roth, M.-P., and Loréal, O. (2004) Strain and gender modulate hepatic hepcidin 1 and 2 mRNA expression in mice. *Blood Cells. Mol. Dis.* **32**, 283–289
61. Brissot, P., Ropert, M., Le Lan, C., and Loréal, O. (2012) Non-transferrin bound iron: A key role in iron overload and iron toxicity. *Biochim. Biophys. Acta BBA - Gen. Subj.* **1820**, 403–410
62. Jenkitkasemwong, S., Wang, C.-Y., Coffey, R., Zhang, W., Chan, A., Biel, T., Kim, J.-S., Hojyo, S., Fukada, T., and Knutson, M. D. (2015) SLC39A14 Is Required for the Development of Hepatocellular Iron Overload in Murine Models of Hereditary Hemochromatosis. *Cell Metab.* **22**, 1–13
63. Marques, L., Auriac, A., Willemetz, A., Banha, J., Silva, B., Canonne-Hergaux, F., and Costa, L. (2012) Immune cells and hepatocytes express glycosylphosphatidylinositol-anchored ceruloplasmin at their cell surface. *Blood Cells. Mol. Dis.* **48**, 110–120
64. Brissot, P. and Loréal, O. (2) Iron metabolism and related genetic diseases: A cleared land, keeping mysteries. *J. Hepatol.* **64**, 505–515
65. Loréal, O., Cavey, T., Bardou-Jacquet, E., Guggenbuhl, P., Ropert, M., and Brissot, P. (2014) Iron, hepcidin, and the metal connection. *Front. Pharmacol.* **5**
66. Cartwright, G. and Wintrobe, M. (1964) Copper metabolism in normal subjects. *Am. J. Clin. Nutr.* **14**, 224–232

Figures legends

Figure 1 : A global location of sgRNA in exon 1 is schematically presented (A) The CRISPR/Cas9 process is depicted in the region around the sgRNA targeted site, in exon 1 of ceruloplasmin gene (B). The resulting mutation selected for our model, and the stop codon occurring in exon 2 due to the frame shift, are also represented (C). The frame shift resulting protein is exhibited and compared to the wild-type sequence (D). Example of agarose gel picture representing the three genotypes used in the present study (E). Blots "a" from $Cp^{+/+}$ rats can be recognized by a band of about 200 bp ; $Cp^{-/-}$ animals are characterized by a lower band "b" of about 150 bp while $Cp^{+/-}$ shows a double-band "c" corresponding to the two alleles. Heteroduplexes are present above $Cp^{+/-}$ bands, as indicated by the white arrow.

Figure 2 : Consequences of the mutation on ceruloplasmin protein and activity, plasma iron bio-availability, and tissue iron concentrations. Plasma ceruloplasmin concentration, n=10 in all groups (A). Total ferroxidase activity, n=10 in all groups (B). Peripheral plasma iron concentration, n=10 in all groups (C). Portal plasma iron concentration, n=10 in $CP^{+/+}$ group, n=9 in $CP^{+/-}$ and $CP^{-/-}$ groups (D). Peripheral plasma transferrin saturation, n=10 in all groups (E). Portal plasma transferrin saturation, n=10 in $CP^{+/+}$ group, n=9 in $CP^{+/-}$ and $CP^{-/-}$ groups (F). Peripheral plasma NTBI concentration, n=10 in all groups (G). Portal plasma NTBI concentration, n=10 in $CP^{+/+}$ and $CP^{-/-}$ groups, n=9 in $CP^{+/-}$ group (H). Hemoglobin concentration, n=10 in $CP^{+/+}$ and $CP^{-/-}$ groups, n=8 in $CP^{+/-}$ group (I). Erythrocyte iron concentration, n=10 in all groups (J). Liver iron concentration, n=10 in all groups (K). Spleen iron concentration, n=10 in $CP^{+/+}$ and $CP^{+/-}$ groups, n=9 in $CP^{-/-}$ group (L). (*, p<0,05 ; **, p<0,01 ; ***, p<0,001)

Figure 3 : Perls staining of liver and spleen. Liver of $CP^{+/+}$ (A) and $CP^{-/-}$ (B) rats. PS : portal space ; CLV : centrolobular vein ; Kupffer cells (example surrounded in black) ; hepatocytes (example pointed with black arrow). Spleen of $CP^{+/+}$ (C) and $CP^{-/-}$ (D), with indication of red pulp (RP) and white pulp (WP).

Figure 4 : Plasma copper concentration, n=10 in all groups (A). Erythrocyte copper concentrations, n=10 in all groups (B). Liver copper concentrations, n=10 in all groups (C). Spleen copper concentrations, n=10 in $CP^{+/+}$ and $CP^{+/-}$ groups, n=8 in $CP^{-/-}$ group (D). Erythrocyte cobalt concentrations, n=10 in all groups (E). Plasma manganese concentrations, n=10 in all groups (F). (*, p<0,05 ; **, p<0,01 ; ***, p<0,001)

Figure 5 : Liver *Hamp* mRNA levels expressed in negative delta cycle threshold, n=10 in all groups (A). Ratio between liver *Hamp* mRNA levels and liver iron concentration, n=10 in all groups (B). Representative examples of liver p-ERK1/2, p-STAT3, and p-SMAD1/5/8 blots with Hsc70 as load control protein (C). Liver *Slc40a1* mRNA levels expressed in negative delta cycle threshold, n=10 in all groups (D). Liver *Heph* mRNA levels expressed in negative delta cycle threshold, n=10 in all groups (E). Representative example of liver ferroportin blots with Hsc70 as load control protein (F). Spleen *Slc40a1* mRNA levels expressed in negative delta cycle threshold, n=10 in all groups (G). Spleen *Heph* mRNA levels expressed in negative delta cycle threshold, n=10 in all groups (H). Representative example of spleen ferroportin and hephaestin blots with Hsc70 as load control protein (I). Duodenum Slc40a1 mRNA levels expressed in negative delta cycle threshold, n=10 in CP+/+ and CP+/- groups, n=9 in CP-/- group (J). Duodenum Heph mRNA levels expressed in negative delta cycle threshold, n=10 in CP+/+ and CP+/- groups, n=9 in CP-/- group (K). Representative example of duodenum ferroportin and hephaestin blots with Hsc70 as load control protein (L). (*, $p<0,05$; ***, $p<0,001$)

Figure 1 part 1

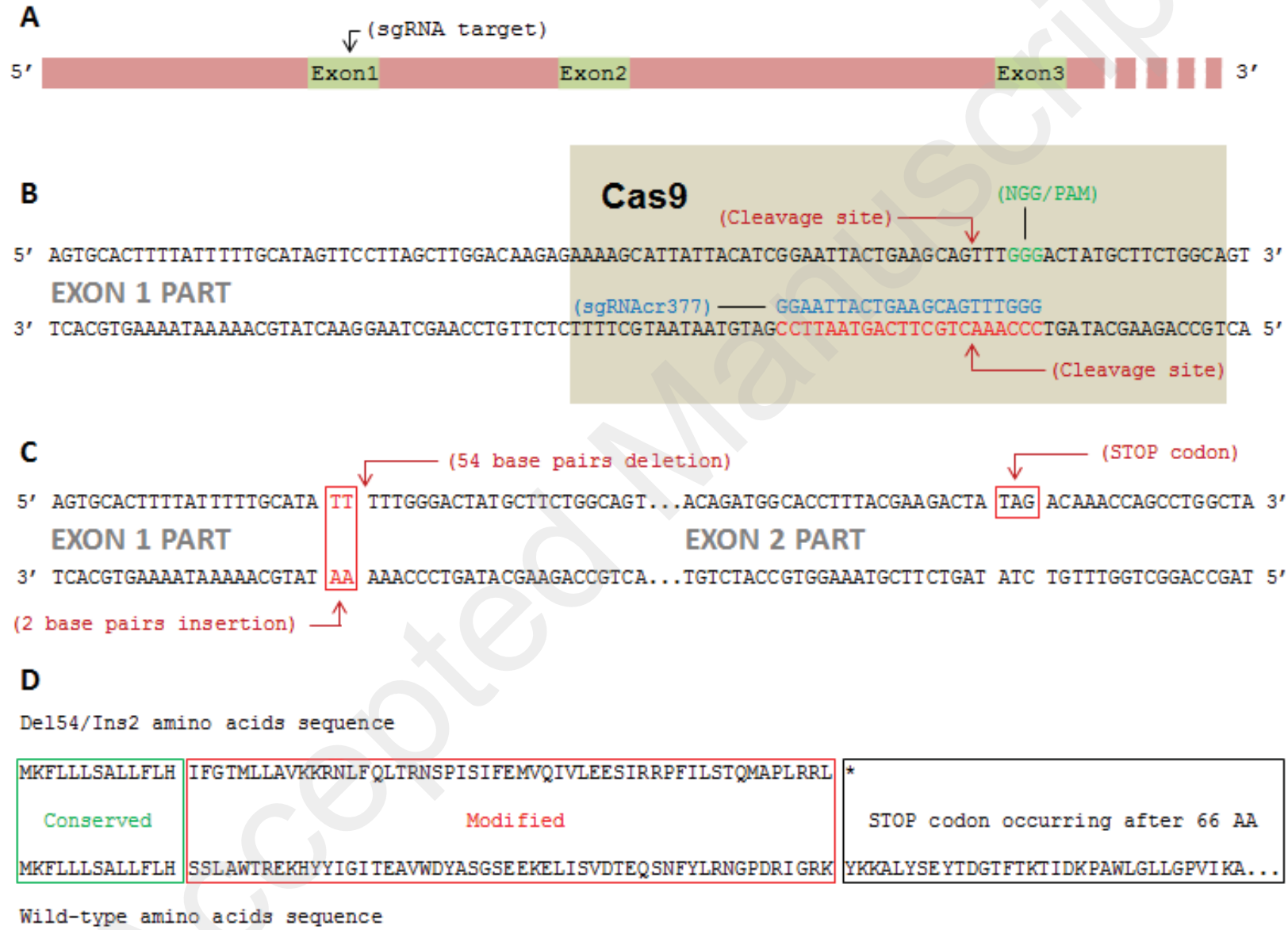

Figure 1 part 2

E

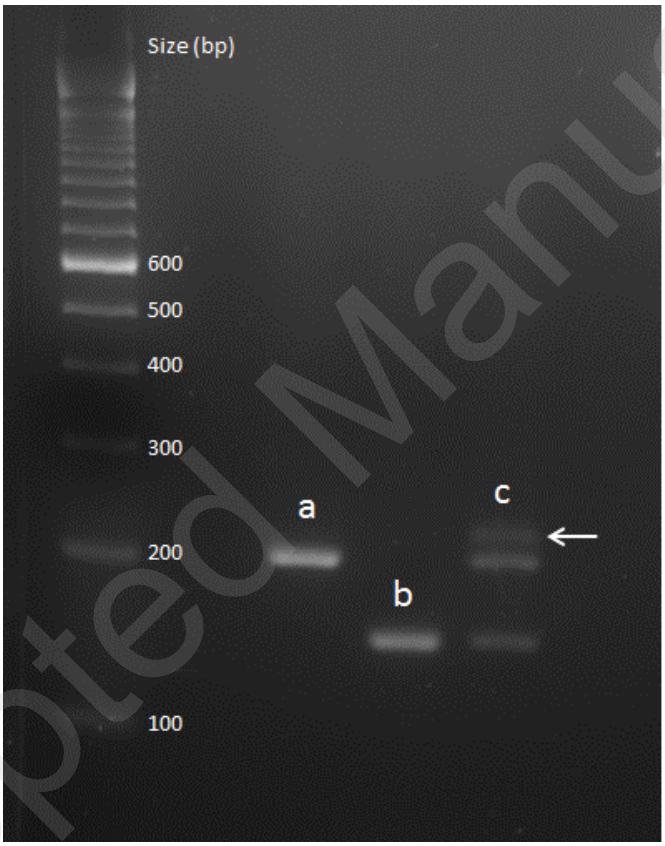

Figure 2

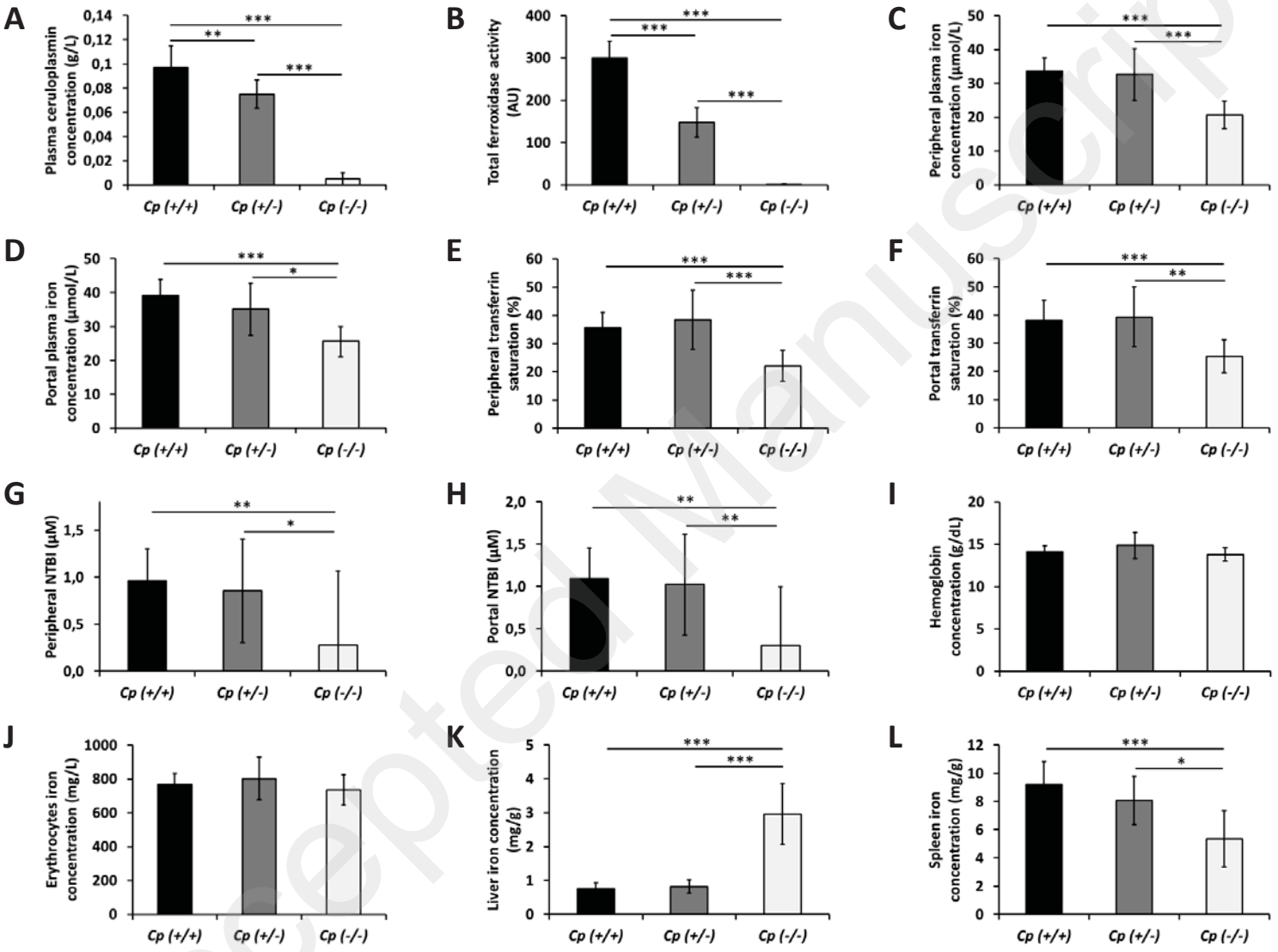

Figure 3

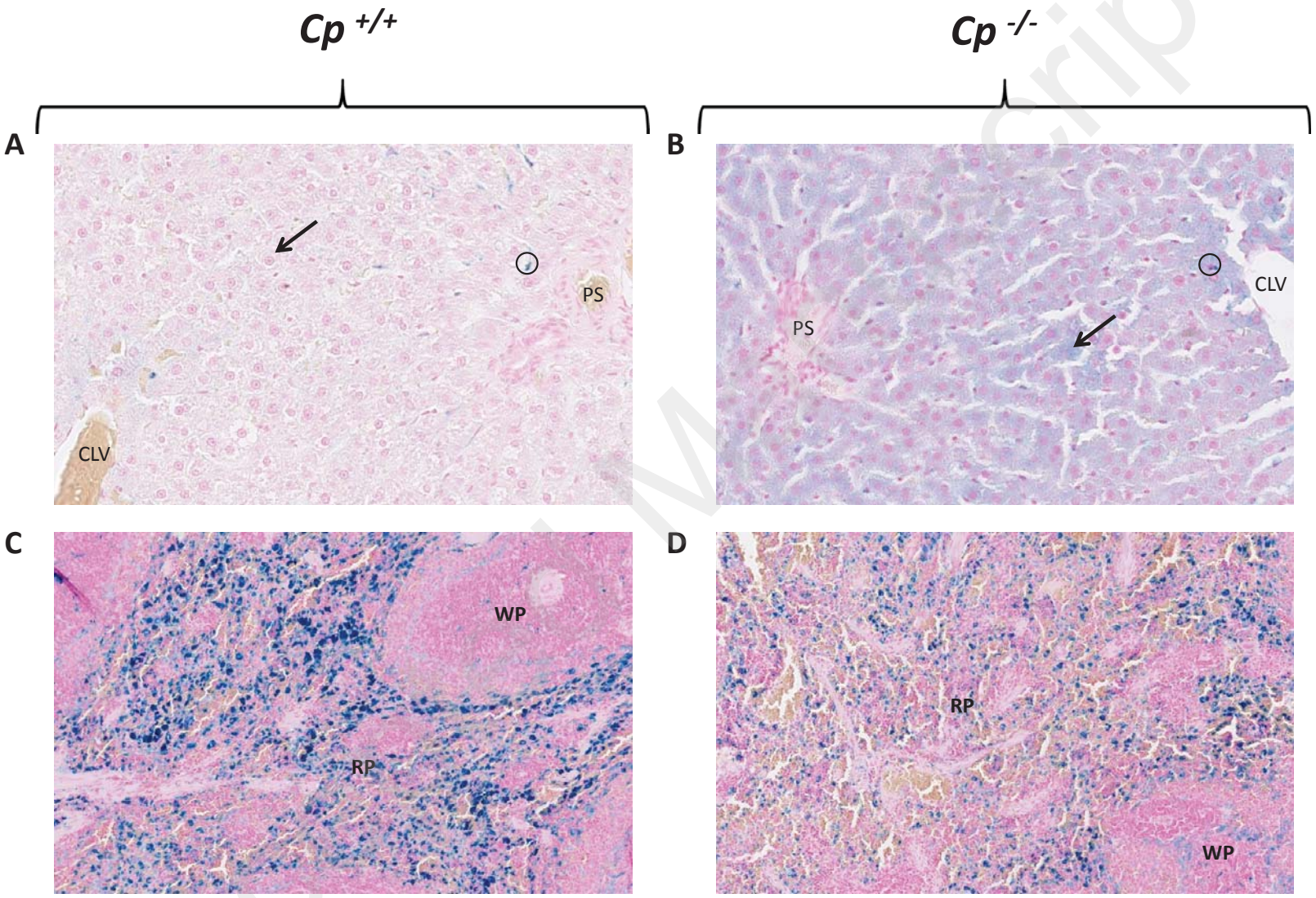

Figure 4

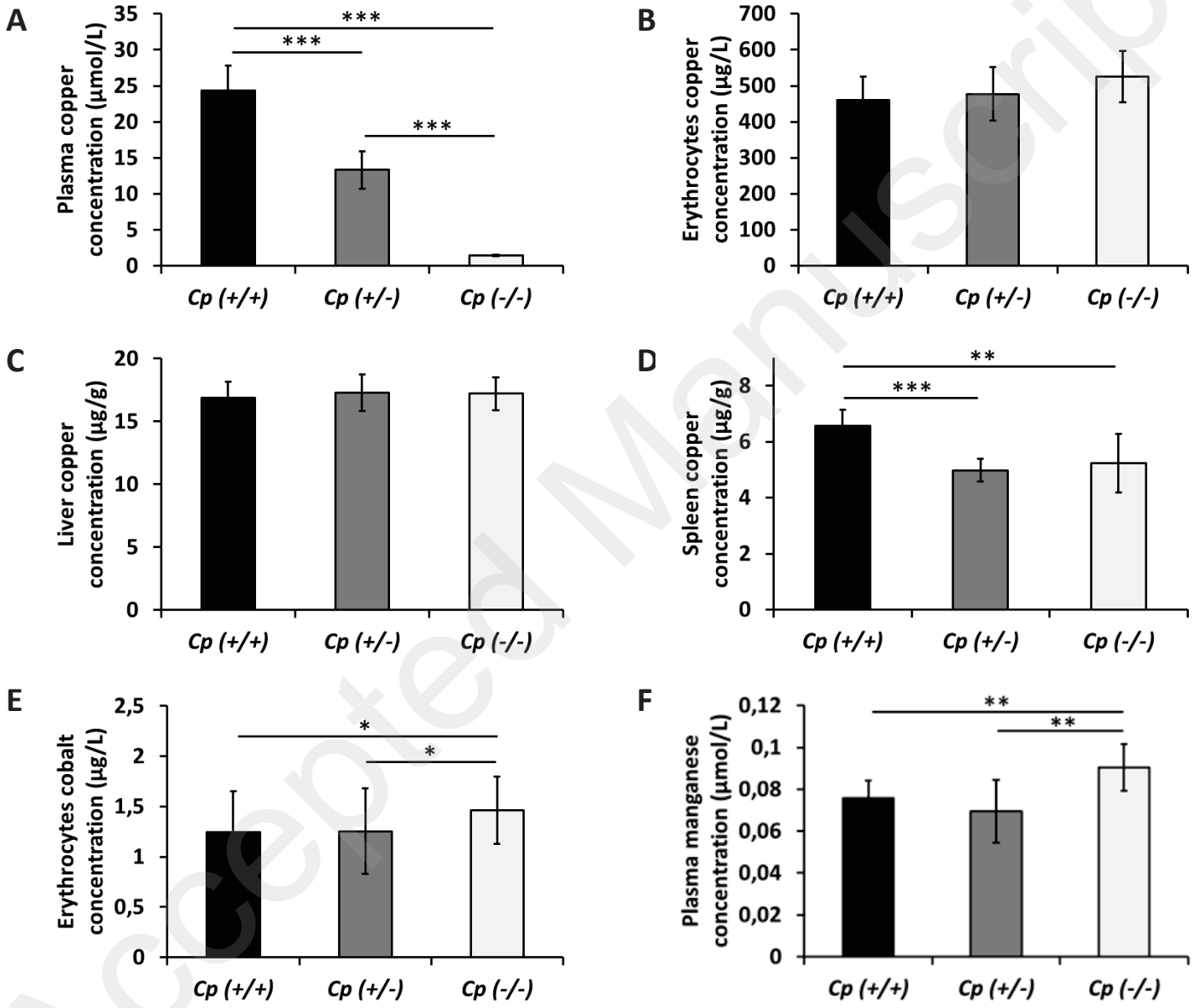

Figure 5c

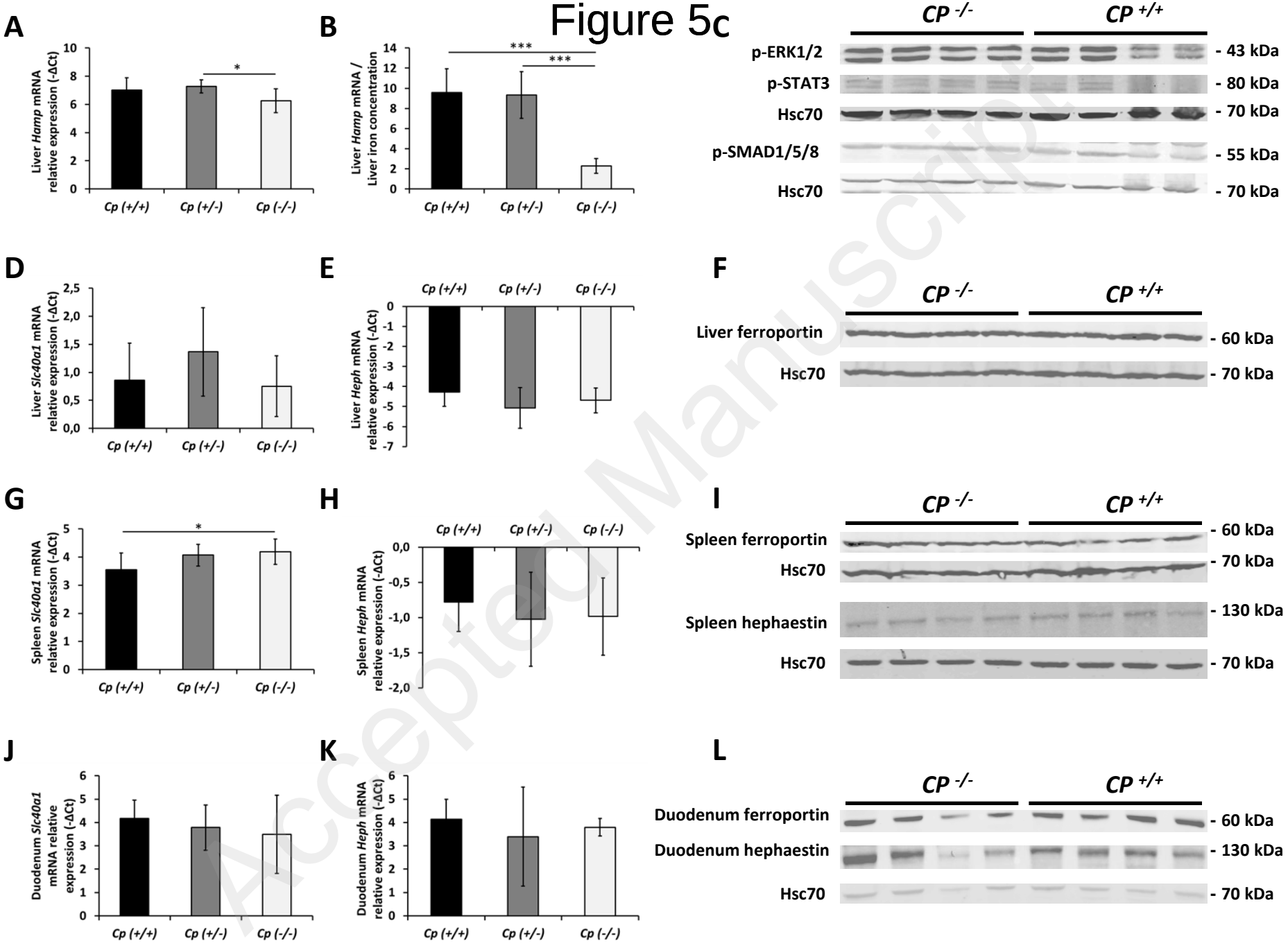

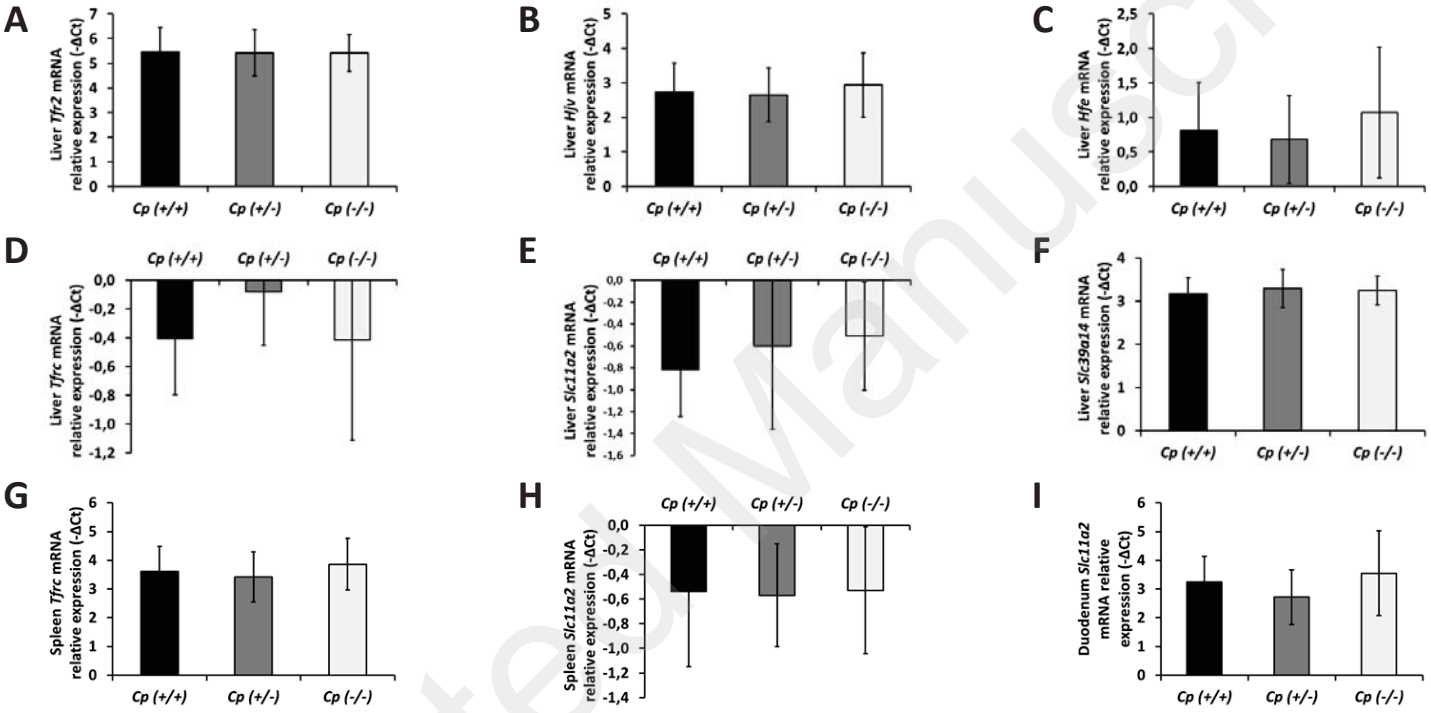

Supplemental data Figure 1 : Liver *Tfr2* mRNA levels expressed in negative delta cycle threshold, n=10 in all groups (A). Liver *Hjv* mRNA levels expressed in negative delta cycle threshold, n=10 in all groups (B). Liver *Hfe* mRNA levels expressed in negative delta cycle threshold, n=10 in all groups (C). Liver *Tfrc* mRNA levels expressed in negative delta cycle threshold, n=10 in all groups (D). Liver *Slc11a2* mRNA levels expressed in negative delta cycle threshold, n=10 in all groups (E). Liver *Slc39a14* mRNA levels expressed in negative delta cycle threshold, n=10 in all groups (F). Spleen *Tfrc* mRNA levels expressed in negative delta cycle threshold, n=10 in all groups (G). Spleen *Slc11a2* mRNA levels expressed in negative delta cycle threshold, n=10 in all groups (H). Duodenum *Slc11a2* mRNA levels expressed in negative delta cycle threshold, n=10 in $CP^{+/+}$ and $CP^{+/-}$ groups, n=9 in $CP^{-/-}$ group (I).

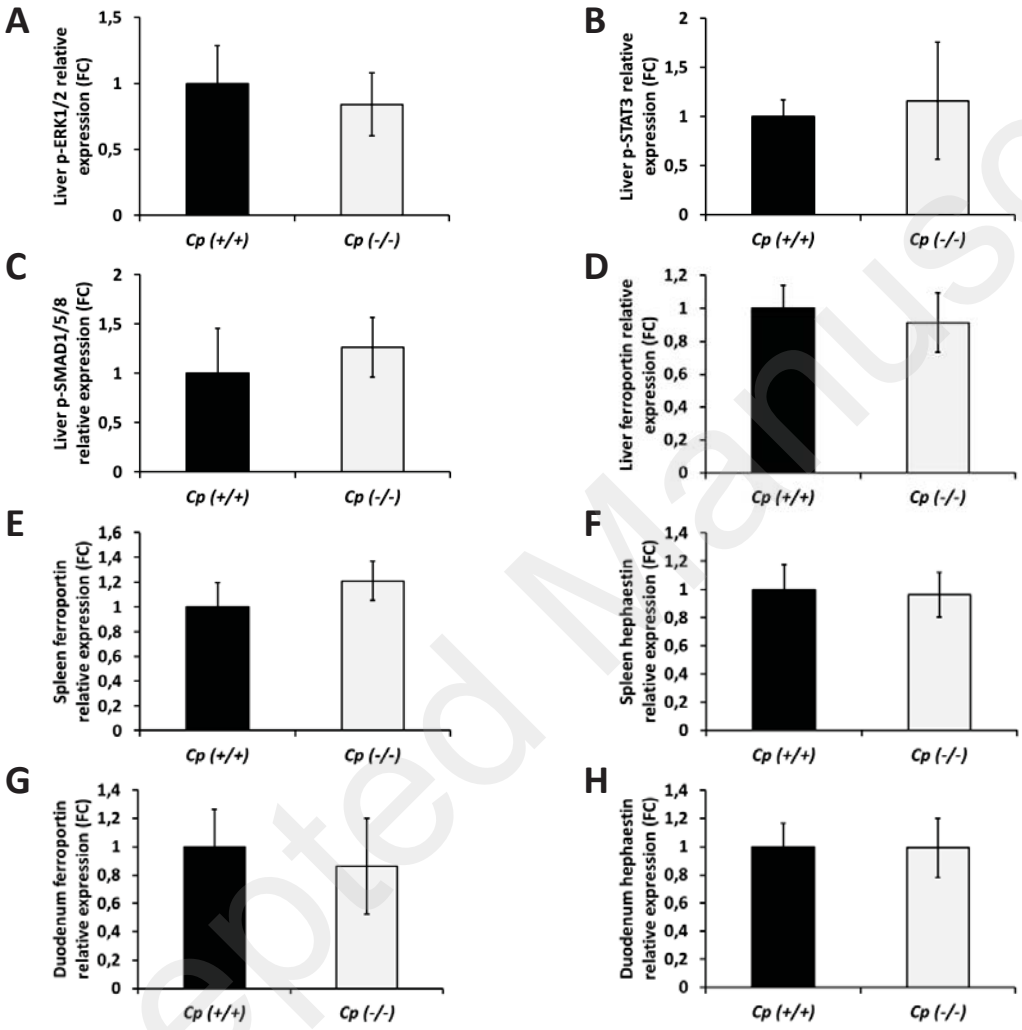

Supplemental data Figure 2 : Liver p-ERK1/2 protein levels expressed in fold-change, n=8 in all groups (A). Liver p-STAT3 protein levels expressed in fold-change, n=8 in all groups (B). Liver p-SMAD1/5/8 protein levels expressed in fold-change, n=8 in all groups (C). Liver ferroportin protein levels expressed in fold-change, n=8 in all groups (D). Spleen ferroportin protein levels expressed in fold-change, n=8 in all groups (E). Spleen hephaestin protein levels expressed in fold-change, n=8 in all groups (F). Duodenum ferroportin protein levels expressed in fold-change, n=7 in $CP^{+/+}$ group, n=6 in $CP^{-/-}$ group (G). Duodenum hephaestin protein levels expressed in fold-change, n=7 in $CP^{+/+}$ group, n=6 in $CP^{-/-}$ group (H).

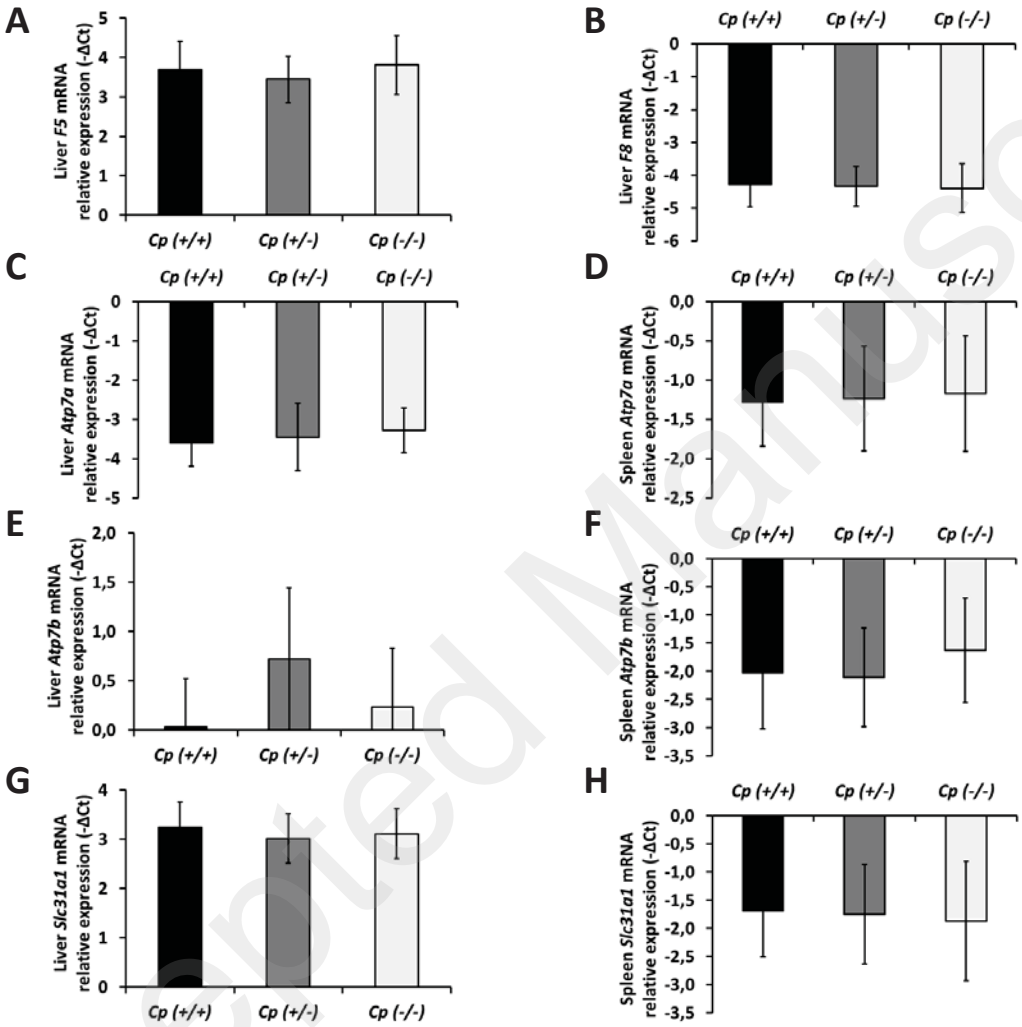

Supplemental data Figure 3 : Liver *F5* mRNA levels expressed in negative delta cycle threshold, n=10 in all groups (A). Liver *F8* mRNA levels expressed in negative delta cycle threshold, n=10 in all groups (B). Liver *Atp7a* mRNA levels expressed in negative delta cycle threshold, n=10 in all groups (C). Spleen *Atp7a* mRNA levels expressed in negative delta cycle threshold, n=10 in all groups (D). Liver *Atp7b* mRNA levels expressed in negative delta cycle threshold, n=10 in all groups (E). Spleen *Atp7b* mRNA levels expressed in negative delta cycle threshold, n=10 in all groups (F). Liver *Slc31a1* mRNA levels expressed in negative delta cycle threshold, n=10 in all groups (G). Spleen *Slc31a1* mRNA levels expressed in negative delta cycle threshold, n=10 in all groups (H).

Gene	Forward primer	Reverse primer
Atp7a	TGGCTGGAACACATAGCGAA	TCCACTTGTTCTTCACTCAGGA
Atp7b	CAAGGTCATCGAGGAAATCGGC	CATGACGGGGATGCCAAACA
F8	TGCCATGGGACTATGTGAGC	TTTGCCGTGTGGAAAAACCG
F5	ATCTATGGGAGGAGGCACGA	TGCGTCTTGGATTGGAACTCA
Gusb	TCGAACAATCGGTTGCAGG	AGCCAATGAAGTTCCGAAGC
Hamp	CTGCAGCCTTGGCATGG	CAGCAGCGCACTGTCATCA
Heph	ATGCACTGCCACGTTACTGA	CTGCAGAATCACAGCTTTTCCA
Hfe	GTGGGATCACCATTTGTGCCAT	ATGCTGCAGGTCACTCACACT
Hjv	TCCTCTTTGTCCAAGCCACC	TCGCCCCCATTGACAGAAC
Hprt1	CTGATTATGGACAGGACTGAAAGAC	CCAGCAGGTCAGCAAAGAACT
Slc11a2	CTTTGTCGTCTCCGTCTTTGC	ATGGGGGCTGCTGCTATTTC
Slc31a1	ACGAGATGATGATGCCTATGACC	AACACTGCCACAAAAGCTCC
Slc39a14	GGCTGGAGGATTTCAGTGTGT	ACCAAACAGCACCAACAGGA
Slc40a1	AGGGACTGGATTGTTGTCGT	GACTGGGGAACCGAATGTCA
Tbp	GGGATTGTACCACAGCTCCA	CAGCAAACCGCTTGGGATTA
Tfrc	AGCTGGACTGCAGGAGACTA	GGGCTGGCAGAAACCTTGAA
Tfr2	CATGTACAACGTGCGCATCA	GGAAAATGTGGCGGAATGGG

Supplemental data Table 1 : Sequences of forward and reverse primers used for real time qPCR.

	$CP^{+/+}$			$CP^{+/-}$			$CP^{-/-}$			
	N	***Mean***	***SD***	***N***	***Mean***	***SD***	***N***	***Mean***	***SD***	***p-value***
Liver molybdenum (µg/g)	10	2,05	0,30	10	2,18	0,29	10	2,09	0,19	*ns*
Liver zinc (µg/g)	10	100,95	10,19	10	101,15	9,68	10	99,86	8,56	*ns*
Liver cobalt (µg/g)	10	0,21	0,16	10	0,16	0,06	10	0,13	0,04	*ns*
Liver manganese (µg/g)	10	7,99	1,18	10	7,71	0,93	10	8,66	0,52	*ns*
Spleen molybdenum (µg/g)	10	0,80	0,14	10	0,72	0,22	8	0,66	0,13	*ns*
Spleen zinc (µg/g)	10	76,59	8,57	10	89,80	34,71	8	77,88	7,59	*ns*
Spleen cobalt (µg/g)	10	0,08	0,03	10	0,06	0,02	8	0,08	0,03	*ns*
Spleen manganese (µg/g)	10	1,04	0,12	10	1,06	0,09	8	0,95	0,10	*ns*
Plasma molybdenum (µmol/L)	10	0,19	0,06	10	0,17	0,03	10	0,18	0,04	*ns*
Plasma zinc (µmol/L)	10	23,31	2,09	10	23,24	3,95	10	22,22	1,97	*ns*
Plasma cobalt (µmol/L)	10	0,03	0,02	10	0,03	0,01	10	0,03	0,02	*ns*
Erythrocytes molybdenum (µg/L)	10	0,59	0,54	10	0,85	1,34	10	0,7	0,67	*ns*
Erythrocytes zinc (µg/L)	10	6960	591,85	10	7337,2	1216,32	10	7004,7	579,59	*ns*

Supplemental data Table 2 : Metal concentrations in liver, spleen, plasma, and erythrocytes. ns : no statistically significant difference.